Brain inflammation in a chronic epilepsy model : evolving pattern of the translocator protein during epileptogenesis

Reference:

Amhaoul Halima, Hamaide Julie, Bertoglio Daniele, Verhaeghe Jeroen, Geerts Elly, van Dam Debby, de Deyn Peter Paul, Kumar-Singh Samir, van der Linden Anne-Marie, Staelens Steven.- Brain inflammation in a chronic epilepsy model : evolving pattern of the translocator protein during epileptogenesis

Neurobiology of disease - ISSN 0969-9961 - (2015), p. 1-14

Full text (Publishers DOI): http://dx.doi.org/doi:10.1016/j.nbd.2015.09.004

Handle/Permalink: http://hdl.handle.net/10067/1283140151162165141

Brain inflammation in a chronic epilepsy model: Evolving pattern of the translocator protein during epileptogenesis

Halima Amhaoul[1], Julie Hamaide[1,2], Daniele Bertoglio[1], Stephanie Nadine Reichel[1], Jeroen Verhaeghe[3], Elly Geerts[4], Debby Van Dam[4], Peter Paul De Deyn[4,5,6], Samir Kumar-Singh[7], Andrew Katsifis[8], Annemie Van Der Linden[2], Steven Staelens[3], Stefanie Dedeurwaerdere[1]

doi: 10.1016/j.nbd.2015.09.004

1. Department of Translational Neurosciences, University of Antwerp, Belgium

2. Bio-Imaging Lab, University of Antwerp, Belgium

3. Molecular Imaging Center Antwerp, University of Antwerp, Belgium

4. Laboratory of Neurochemistry and Behaviour, University of Antwerp, Belgium

5. Department of Neurology and Memory Clinic, Hospital Network Antwerp (ZNA) Middelheim and Hoge Beuken, Belgium

6. *Department of Neurology and Alzheimer Research Center, University of Groningen and University Medical Center Groningen (UMCG), The Netherlands*

7. Laboratory of Cell Biology & Histology, University of Antwerp, Belgium

8. Department of PET and Nuclear Medicine, Royal Prince Alfred Hospital, Australia

Corresponding author:

Stefanie Dedeurwaerdere

Department of Translational Neurosciences, University of Antwerp, FGEN CDE T4.98, Universiteitsplein 1, Wilrijk, Antwerp 2610, Belgium

Phone number: +3232652638

stefanie.dedeurwaerdere@uantwerpen.be

Short running title:

Temporal TSPO expression in the limbic system in epilepsy

Keywords:

Epilepsy, seizure, brain- and neuroinflammation, translocator protein or peripheral benzodiazepine receptor, microglia, ^{18}F-PBR111 PET

Abstract

Aims: A hallmark in the neuropathology of temporal lobe epilepsy is brain inflammation which has been suggested as both a biomarker and a new mechanistic target for treatments. The translocator protein (TSPO), due to its high upregulation under neuroinflammatory conditions and the availability of selective PET tracers, is a candidate target. An important step to exploit this target is a thorough characterisation of the spatiotemporal profile of TSPO during epileptogenesis.

Methods: TSPO expression, microglial activation, astrocyte reactivity and cell loss in several brain regions were evaluated at five time points during epileptogenesis, including the chronic epilepsy phase in the kainic acid-induced *status epilepticus* (KASE) model (n= 52) and control Wistar Han rats (n= 33). Seizure burden was also determined in the chronic phase. Furthermore, ^{18}F-PBR111 PET/MRI scans were acquired longitudinally in an additional four KASE animals.

Results: TSPO expression measured with *in vitro* and *in vivo* techniques was significantly increased at each time point and peaked two weeks post-SE in the limbic system. A prominent association between TSPO expression and activated microglia (p<0.001; r=0.7), as well as cell loss (p<0.001; r=-0.8) could be demonstrated. There was a significant positive correlation between spontaneous seizures and TSPO upregulation in several brain regions with increased TSPO expression.

Conclusions: TSPO expression was dynamically upregulated during epileptogenesis, persisted in the chronic phase and correlated with microglia activation rather than reactive astrocytes. TSPO expression was correlating with spontaneous seizures and its high expression during the latent phase might possibly suggest being an important switching point in disease ontogenesis which could be further investigated by PET imaging.

List of Abbreviations

3-D	Three-dimensional
CA	Cornu ammonis
CT	Computed tomography
DG	Dentate gyrus
DH	Dentate hilus
GFAP	Glial fibrillary acid protein
KA	Kainic acid
KASE	Kainic acid-induced *status epilepticus*
MR	Magnetic resonance
MRI	Magnetic resonance imaging
OD	Optical density
PBS	Phosphate buffered saline
PET	Positron emission tomography
ROI	Region of interest
s.c.	Subcutaneous
SE	*Status epilepticus*
SRS	Spontaneous recurrent seizures
TLE	Temporal lobe epilepsy
TSPO	Translocator protein
vEEG	Video-electroencephalography
VOI	Volume of interest

Introduction

Epilepsy is one of the most common chronic neurological disorders with an estimated prevalence of about 65 million people worldwide (Ngugi et al., 2010). It has a devastating impact on the patients' everyday life as it is characterised by spontaneous recurrent seizures (SRS) due to aberrant neuronal excitation. The medicinal therapies available are purely symptomatic, have significant side effects and are ineffective in up to 30% of the patients. Furthermore, the neurobiological processes that result in (acquired) epilepsy remain unclear, which strongly impedes the development of more potent, targeted and efficient treatments. Interestingly, immune-challenging insults like fever, infection and trauma, are associated with the acute occurrence of seizures and with a higher risk of developing epilepsy later in life (Ravizza et al., 2011; Vezzani et al., 2011). In addition, recent studies have demonstrated that a vast number of different inflammatory mediators are present in both human as well as preclinical resected epileptic brain tissue. Moreover, insults triggering epileptogenesis can cause an immediate upregulation of inflammatory processes in the affected brain areas (Friedman et al., 2009; Dedeurwaerdere et al., 2012b). As a result, it has been demonstrated that brain inflammation can be regarded as both cause and consequence of epileptic seizures. Given that inflammation may be an important factor in the reorganisation of a normal neuronal network into an epileptic one, this offers a new target for the development of therapies and diagnostic tools. Nevertheless, brain inflammation constitutes both beneficial and detrimental aspects. More specifically, innate defensive mechanisms are believed to safeguard the organism from invading pathogens or insults while chronic inflammation is believed to have a negative impact on disease. Due to this complex nature of inflammation it is of vital importance to understand the inflammation context that is created during disease and to characterise the broad spectrum of molecules and processes involved (Dedeurwaerdere et al., 2012a; Amhaoul et al., 2014). These fundamental insights are necessary to completely understand the role of brain inflammation in the pathophysiology of epilepsy, to fully profit from the potential of anti-inflammatory strategies and to explore the possibilities of using inflammation as a potential biomarker (Amhaoul et al., 2014).

A potential candidate biomarker is the translocator protein (TSPO) (Dedeurwaerdere et al., 2012a). This protein, previously known as the peripheral benzodiazepine receptor, prominently features in brain tissue of patients with temporal lobe epilepsy (TLE). TSPO is normally present in low concentrations in glial cells, but upon activation of these cells, it becomes significantly upregulated. Although this indirect relation between brain inflammation and TSPO has been known for several decades, the actual progression of TSPO expression during epileptogenesis has not been fully described. In addition, its role in disease ontogenesis and progression still remains elusive. Therefore, to disentangle the functional implications of TSPO up to the molecular mechanistic level and to elucidate whether TSPO could be a valid biomarker for epilepsy, firstly requires a clear understanding of the spatial expression pattern of TSPO during the different stages of pathology.

Kainic acid-induced *status epilepticus* (KASE) in rats is a well-established model for TLE, which is the most common and refractory form of focal, acquired epilepsy in adults. In this model, epileptogenesis is triggered by the *status epilepticus* (SE). After a latent period, which is not per se a silent period and cannot be exactly outlined in time, SRS occur. With this study, we firstly characterised the spatiotemporal profile of TSPO *post-mortem* in the rat brain of the KASE model using a cross-sectional study design. Secondly, we assessed the relationship of TSPO with other pathologic hallmarks of the KASE model, namely neuronal cell loss and glial activation. Thirdly, the epileptic outcome, namely SRS, was determined during the chronic period as well as its relationship with TSPO expression. Finally, we followed-up TSPO expression longitudinally and three-dimensionally (3-D) using *in vivo* imaging of TSPO with ^{18}F-PBR111 positron emission tomography (PET).

Materials and methods

Animals

Seven week old male Wistar Han rats (Charles River Laboratories, France) were single housed under a 12 h light/dark cycle, in a temperature and humidity controlled environment. Food and water were available *ad libitum.* Animals were allowed five days of acclimatization to the animal facilities before the start of the experiments and were treated in accordance with the guidelines approved by the European Ethics Committee (decree 86/609/CEE) and the Animal Welfare Act (7 USC 2131). All animal experiments were approved (ECD 2014-39) by the ethical committee of the University of Antwerp (Belgium).

Study design

To study TSPO expression, glial activation and cell loss during epileptogenesis and established epilepsy, control and KASE animals were sacrificed at five crucial time points in disease progression: i.e. 2 days (early phase), 1 week (latent phase), 2 weeks (latent phase), 6 weeks (transition phase) and 3 months (chronic phase) post-SE. At the start of the experiments, the number of animals for the first three time points was 4 to 6 for the control and 6 to 9 for the KASE group. A higher number of animals were included in the groups of the 6 weeks and 3 months' time points as seizure burden by means of video-electroencephalography (vEEG) was assessed in these subjects (control *n*= 7-12; KASE *n*= 12-14). To assess whether the implantation of the electrodes itself would cause brain inflammation, a subset of animals (control *n*= 3, KASE *n*= 2) included in the 3 months' time point were not implanted. No differences could be demonstrated between animals that underwent surgery and those who did not for all studied histology variables, and thus were included in the analysis. Upon termination of the experiment, brains were dissected for histological investigation.

A descriptive PET investigation was executed to illustrate the results of the cross-sectional study *in vivo* and to assess the feasibility of measuring TSPO upregulation longitudinally in rats with a non-

invasive, previously validated protocol (Dedeurwaerdere et al., 2012a). For this, four KASE animals were repeatedly scanned 2 and 4 weeks post-SE by means of ^{18}F-PBR111 PET. An additional scan 6 weeks post-SE was only available for two out of the four animals. A control animal was scanned 2 weeks post-sham SE. Magnetic resonance imaging (MRI) scans were taken in parallel for co-registration purposes.

Induction of SE in the KASE model

The animals were repeatedly administered low-dose subcutaneous (s.c.) injections of kainic acid (KA; initial dose 5 mg/kg – subsequent doses 2.5 mg/kg; A.G. Scientific, USA), as this method has proven both its efficacy and low mortality rate, while controls received saline injections (Dedeurwaerdere et al., 2012a). Importantly, this protocol allows for each individual animal to receive a personalized dose of KA, thus rendering the proconvulsant less lethal.

At SE induction, the rats were aged 7.5 weeks weighing 222 ± 1.8 g for the control animals (*n*= 33) and 224 ± 1.7 g for the KASE group (*n*= 56). About 45 min after the initial KA injection (5 mg/kg, s.c.) repetitive injections of 2.5 mg/kg were given every half an hour unless the rats showed non-convulsive epileptic behaviour. In that case, the injections were delayed and stopped when convulsive seizures started. During the entire induction period, the animals were continuously observed and after 4 h of SE, diazepam (4 mg/kg; NV Roche SA, Belgium) was administered intraperitoneally to arrest the seizures. All, but three KASE animals of the 2 days' time point, reached SE after receiving an average dose of 13.6 ± 0.91 mg/kg KA. Control animals received a saline injection. To prevent dehydration, Hartmann's solution (10 ml/kg, s.c.; Viaflo Baxter Healthcare, Belgium) was administered at the end of the procedure. Additional care was taken the days following SE by providing the animals with enriched soft food pellets and Hartmann's solution. One animal died during SE, while two others died the first day post-SE (5.4 % mortality rate). These animals belonged to the 6 weeks' time point and were excluded from analysis. In addition, the three animals that did not reach SE were also excluded from the study.

vEEG

EEG-electrode implantation

This procedure was performed in anesthetized animals (isoflurane: 5% induction, 2.5% maintenance; Forene, Belgium) two weeks before the start of the vEEG recordings, guaranteeing an adequate recovery. Six bilateral epidural electrodes were implanted: two frontal, two parietal and two occipital (right= reference, left= ground) according to van Raay et al. (2009). These electrodes were fixed into a plastic plug (Bilaney consultants, Plastics one Inc., UK) and secured to the skull using dental cement (Simplex Rapid, Kemdent, UK; Durelon, 3M ESPE, USA). At the end of the surgery, local administration of xylocaine (2%; AstraZeneca, Belgium) and injection of buprenorphine (0.01 mg/kg, s.c.; Ecuphar, the Netherlands) was given for pain relief, as well as Hartmann's solution to prevent dehydration (10 ml/kg, s.c.). Animals were returned to their home cages for recovery while kept warm.

vEEG recording and analysis

A total of 100 h of vEEG data was collected directly before sacrification from freely moving control and KASE rats. The animals were connected via a six-channel cable (Plastics One Inc., USA) to a swivel and six-channel commutator (Plastics One Inc., USA). The commutator was connected to the digital EEG acquisition system (Brain-lab Measure Station, OSG bvba, Belgium; Ponemah P3 Plus, Data Sciences International, USA). The camera (Sony Handycam DCR-HC51E, Sony Corporation, Japan; Axis P1353, Axis Communications, Sweden), used to record synchronized video, was positioned above the cages allowing simultaneous visualisation of four animals. An additional night vision infrared LED light bar was installed to enable recordings during the dark period.

Analysis was performed manually using BrainRT^{TM} (OSG bvba Rumst, Belgium) or Ponemah P3 Plus software (Data Sciences International, USA). Identification of SRS was based on previously defined criteria (van Raay et al., 2009; Williams et al., 2009; White et al., 2010; Dedeurwaerdere et al., 2011).

Briefly, a seizure was recognised on EEG as a signal with an amplitude of at least three times baseline signal and evolving peak frequency which persists for at least five seconds. In addition, to be classified as epileptic activity, the severity of the SRS based on the behavioural scale of Racine (Racine, 1972) was determined by the video-recordings.

Histology

At each time point, the animals were sacrificed by rapid decapitation and brains were immediately removed from the skull. If the animals were monitored by vEEG, they were sacrificed directly thereafter. All right hemispheres were directly fresh-frozen in 2-methylbutane (VWR, USA) at -35°C and were preserved at -80°C. The left hemispheres were fixed in 4% paraformaldehyde (VWR, USA) overnight and were subsequently drenched in 20% sucrose solution enriched with 0.1% sodium azide (VWR, USA) for another 24 h. In turn, the fixed tissue was snap-frozen in 2-methylbutane at -40°C and stored at -80°C. Serial coronal sections (20 µm) were collected at -3.24 mm (dorsal hippocampus) and at -10.20 mm (cerebellum) from bregma (Paxinos and Watson, 2007), in triplicate, on coated glass slides using a cryostat (Leica, Germany). One control animal of the 6 weeks group was not dissected out properly and therefore excluded from further processing.

Immunohistochemistry

Nissl and NeuN staining

Cresyl violet staining, also known as the nissl staining, was performed on freshly-frozen cryosections to visualise cell loss. However, it does not exclusively stain neurons and therefore a NeuN staining was additionally performed for quantification purposes. NeuN is a neuronal nuclear antigen which is used as a marker for neurons. Briefly, cryosections were dried and washed using phosphate buffered saline (PBS). Next, non-specific binding was blocked using 0.5% Triton X-100 and 0.05% normal horse serum in PBS. Subsequently, the sections were incubated overnight with the primary antibody against NeuN (mouse anti-rat; 1:2000; Merck Millipore, Germany) in antibody diluent containing

0.5% Triton X-100 and 0.05% normal horse serum. The next morning, sections were washed prior to being incubated for 2 h with peroxidase-conjugated secondary antibody (donkey anti-mouse; 1:500; Jackson Immunoresearch, UK). Finally, in order to visualise the binding, sections were exposed to the colorimetric diaminobenzidine staining.

NeuN was scored visually in accordance to Dedeurwaerdere et al. (2013) on images taken at a 4x magnification in the hippocampal subregions cornu ammonis (CA) 1, CA3, CA4 and dentate hilus (DH). The score for the hippocampus was obtained by the composite score of its subregions. The cell score, which represents the cell density, ranged from 4 (normal) over 3 (some cell loss), 2 (obvious cell loss) and 1 (severe cell loss) to 0 (no cells and total destruction of normal tissue architecture) (Supplementary figure 1). All scoring was done blinded for treatment by three different investigators on triplicate sections of which the mean score was used for statistical analysis. The cresyl violet staining was only used for visualisation purposes.

OX-42 and ED-1 staining

Microglia were visualised by immunohistochemical staining against both the CD11b- (OX-42) and CD68-receptor (ED-1), which were carried out as previously described (Van den Eynde et al., 2014). The CD11b-receptor is also known as the complement receptor 3 and is a macrophage associated marker expressed by all microglia (Saijo and Glass, 2011) where it becomes upregulated upon inflammation (Noda and Suzumura, 2012). The CD68-receptor is a member of the scavenger receptor family, which is predominantly expressed in macrophages, neutrophils and activated microglia on the lysosomes, endosomes and to a lesser extent on the cell surface (Patel et al., 2013). Thus it will give insights into the presence of activated, phagocytic microglia. Both markers can also stain macrophages.

OX-42 staining was evaluated semi-quantitatively on fixed cryosections in the CA1, CA3, CA4, DH, amygdala, piriform cortex, (parietal) cortex, thalamus, cerebellum and pons. The score for the hippocampus was obtained as the composite score of its subregions. The scoring was done in

accordance with Missault et al. (2014). Briefly, a categorical ranking scale based upon cell morphology (0 – resting microglia; 1 – more resting than activated microglia; 2 – predominantly activated microglia) and density of cells (0 – low density; 1 – high density, individual cells can still be distinguished; 2 – high density, individual cells cannot be delineated) was performed microscopically (20x magnification) and blinded for treatment (Supplementary figure 1). A summation of both scores and eventually the mean of the triplicate was calculated for statistical analysis. ED-1 staining was also assessed semi-quantitatively on fresh-frozen cryosections and blinded for treatment in the same regions according to Sharma et al. (2008). Briefly, an estimation of the number of ED-1-positive cells was made at a 40x magnification in triplicate, so that eventually a score ranging from 0 to 5 was assigned with a score of 0 indicating no ED-1-positive cells in the respective region and a score of 5 indicating more than 80 ED-1-positive cells (Supplementary figure 1).

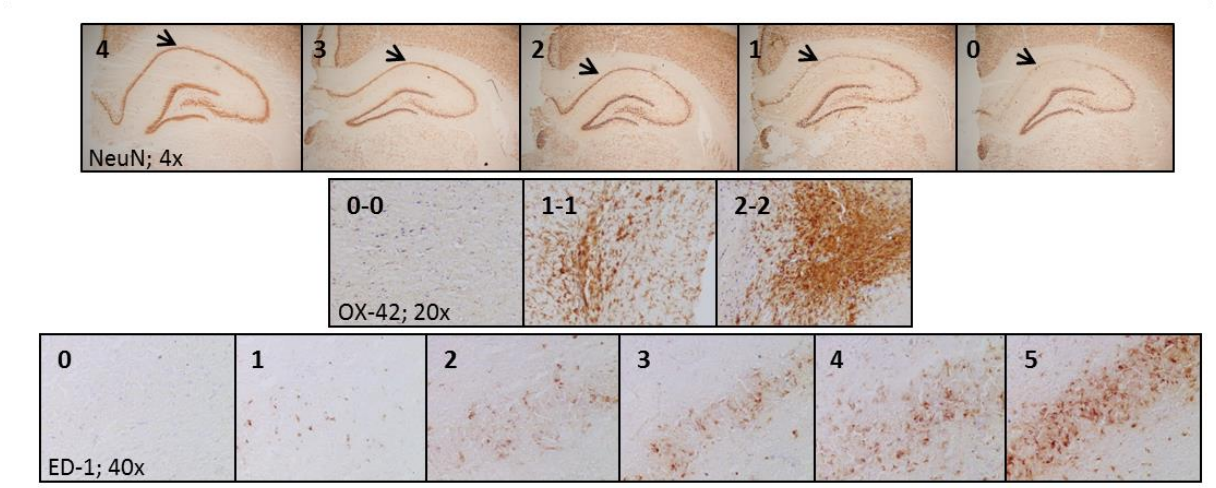

Supplementary figure 1. Visual representation of the semi-quantitative scoring of the NeuN, OX-42 and ED-1 staining. Each row of images represents a different staining. For the NeuN staining the CA1 region (arrow) of the hippocampus is scored as an example. The score ranges from 4 to 0, with 4 indicating normal cell tissue architecture and 0 total destruction. For the OX-42 staining, the amygdala is scored as an example, with 0-0 indicating the normal situation while 2-2 indicates the most severe condition with an extreme high density of amoeboid microglia. Finally, the ED-1 scoring is exemplified in the CA1 region of the hippocampus, with 0 indicating no ED-1 positive cells at all, while 5 indicates a very high number of ED-1 positive cells.

GFAP staining

Visualisation of the involvement of reactive astrocytes was done by immunohistochemical staining of the glial fibrillary acid protein (GFAP), which is an important intermediate filament protein and is upregulated upon activation of astrocytes. Briefly, fixed cryosections were dried and washed using PBS. Next, non-specific binding was blocked using 3 % hydrogen peroxide followed by 10 % normal goat serum in 10 % milk. Subsequently, the sections were incubated overnight with the primary antibody against GFAP (rabbit anti-rat; 1:1000; Dako, Denmark) in antibody diluent containing 10 % normal goat serum and 10 % milk. The next morning, sections were washed prior to being incubated for 1 h with biotinylated secondary antibody (goat anti-rabbit; 1:200; Jackson Immunoresearch, UK). Finally, in order to visualise the binding, sections were first exposed to ExtraAvidin peroxidase before the colorimetric diaminobenzidine staining was applied.

GFAP staining was evaluated semi-quantitatively and blinded to treatment according to Sharma et al. (2008) in the same regions as assessed for the microglial markers. The same scoring strategy was used as for the ED-1 staining.

Autoradiography

TSPO expression was detected by *in vitro* autoradiography with ^{3}H-PK11195 (PerkinElmer, USA); a selective radiolabelled ligand of TSPO which directly binds to this receptor with high affinity (Le Fur et al., 1983; Pike et al., 1993). Briefly, in order to assess the total ligand-receptor binding, fresh-frozen cryosections were dried and incubated in 50 mM Tris-HCl buffer containing 1 nM ^{3}H-PK11195 at room temperature for 30 min. Consecutive sections underwent an identical incubation process, with the extension that also non-labelled PK11195 (Sigma-Aldrich, USA) was added to the radioligand solution in excess (20 µM), so that non-specific binding could also be determined. Subsequently, the sections were washed with buffer and distilled water to remove the excess of unbound tracer. All sections and a ^{3}H-standard (for calibration; American Radiolabeled Chemicals Inc., USA) were exposed to an Amersham Hyperfilm MP (GE Life Sciences, Belgium) for an exposure time of 8 weeks.

After the exposure period had passed, films were developed manually. Finally, the autoradiographic films were digitalized by an Epson V700 photo scanner (Seiko Epson Corporation, Japan).

Specific binding of TSPO was quantitatively measured in the following regions of interest (ROIs): (parietal) cortex, corpus callosum, CA1, CA2, CA3, dentate gyrus (DG), amygdala, entorhinal cortex, piriform cortex, thalamus, hypothalamus and cerebellum. The hippocampus as a whole was assigned a value corresponding to the sum of all its subregions. All ROIs were delineated manually in triplicate both on the total and non-specific binding sections using ImageJ (National Institute of Health, USA). In order to quantify TSPO expression, the optical density (OD) for each ROI was converted to doses of radioactivity (Bq/mg tissue) with the ^{3}H calibration values in GraphPad Prism 6 (GraphPad Software Inc., USA). The specific binding of the radioligand was determined (in grey values) by subtracting the non-specific binding from the total binding.

On the autoradiograms, it seemed that within some ROIs there was a more localised binding. This was quantified using the threshold tool of ImageJ (National Institute of Health, USA), which was visually set to include only the area of increased TSPO specific binding. The area with an OD above the threshold was determined as a percentage of the total ROI. In addition, the total ^{3}H-PK11195 binding in that area was measured. For this analysis only the KASE rats were included as there were no focal areas with elevated TSPO in the control rats. The TSPO focal binding and the TSPO % area values were statistically analysed further.

Longitudinal *in vivo* brain imaging using ^{18}F-PBR111 PET and T_2 MRI

^{18}F-PBR111 radiosynthesis was performed according to Dedeurwaerdere et al. (2012a). PET scanning was executed at the Molecular Imaging Center Antwerp on an Inveon PET/computed tomography (CT) scanner (Siemens Preclinical Solution, USA) and physiological monitoring was performed as previously described (Dedeurwaerdere et al., 2012a). Rats were anesthetised using isoflurane in medical oxygen and scanned for 60.7 min. Thirty seconds after start of the scan, the radiotracer (injected dose 9.62 ± 1.65 MBq, specific activity 124.3 ± 18.1 GBq/µmol, cold mass 0.08 ± 0.004 nmol

or 0.35 nmol/kg in a volume of 0.5 ml) was administered into the tail vein over a duration of 1 min with an automated pump (Pump 11 Elite, Harvard Apparatus, USA) and a glass syringe (Model 1001 LT SYR, Hamilton Company, USA). An arterial blood sample was taken 50 min after the start of the scan for metabolite analysis according to Katsifis et al. (2011). After the PET scan, a 10 min 80 kV/500 µA CT scan was performed for attenuation correction.

List mode PET data were sorted into 28 frames (60.7 min; frames: 8 x 15 s, 6 x 20 s, 6 x 60 s, 3 x 180 s, 5 x 500 s). Iterative image reconstruction was accomplished by fourier rebinning (Defrise et al., 1997) followed by 4 iterations of two-dimensional ordered-subset expectation maximization algorithm (Hudson and Larkin, 1994) using 16 subsets provided by the manufacturer. Normalization, dead time correction, random subtraction, CT-based attenuation, and single-scatter simulation scatter corrections were applied.

In the same week as the PET/CT scans were acquired, MRI scanning was performed at the Bio-Imaging Lab of the University of Antwerp. The animals were anesthetized using isoflurane in a mixture of N2/O2 and placed in prone position into the scanner (9.4T Biospec, Bruker, Germany) with the head fixed in a head holder. After the Tripilot scout images, a rapid acquisition with relaxation enhancement sequence was used to obtain 70 coronal slices with a 0.4 mm thickness. Other imaging parameters were: TR/TE= 8283.5 ms/33.5 ms; acquisition matrix= 256 x 344; field of view= (30 x 40 x 28) mm^3; resolution= (0.17 x 0.114 x 0.35) mm^3). The magnetic resonance (MR) image acquisition procedure lasted for about 10 min after which the animals were placed in a recovery box. All image data were acquired using ParaVision 5.1 (Bruker, Germany).

Coregistration of PET and MRI was performed by automated rigid matching of CT and MR images using PMOD software (PMOD Technologies, Switzerland). Since PET and CT were acquired sequentially on the same bed, the CT to MR transformation was used to overlay the PET and MR images. For each animal, volumes of interest (VOIs) were individually delineated on the MR images, since structural abnormalities were present in post-SE animals (PMOD software, PMOD Technologies,

Switzerland). The relevant VOIs included the olfactory bulb, frontal cortex, hippocampus, amygdala, insular cortex, entorhinal cortex, piriform network (rostral part of the piriform cortex and endopiriform nucleus), thalamus, hypothalamus, ventricles and cerebellum. Raw data statistics were generated with PMOD for further analysis. The ratio between the VOI activity and the metabolite-corrected plasma activity (50' ratio) (PET) according to Dedeurwaerdere et al. (2012a) and volumes (MRI) were determined.

Statistical analysis

Data in some of the groups were not normally distributed, and therefore all data were analysed using non-parametric tests. The Mann-Whitney U test was performed to determine differences between control and KASE animals at each time point for all histology variables. The Spearman's rank correlation test was used to investigate the relationship within KASE animals between TSPO binding on the one hand and the histology variables on the other hand. This was executed on the composite score for the hippocampus. The correlations for the separate time points did not yield additional information, therefore, to increase statistical power all time points were analysed together. The temporal changes of the histology variables were studied for the KASE animals using a Kruskal-Wallis test with a post-hoc Dunn's multiple comparisons test. Each comparison was made to the time point with the highest value. For this statistical analysis, the OX-42 and GFAP score needed to be normalized because these two variables showed fluctuations in the control group. This was done by subtracting the mean value of the corresponding control group from each value in the KASE group. Finally, a Spearman's rank correlation test was used to investigate the relationship within KASE animals between the number of SRS per day and the TSPO binding. For this correlation an in house dataset (n= 9) was added to increase statistical power. Importantly, all these animals were treated in the same way as the animals of this study. All analyses were done using Graphpad Prism 6, except for the Mann-Whitney U test which was done using SPSS (IBM SPSS Statistics 20, USA). Statistical significance was set at $p \leq 0.05$.

Results

TSPO upregulation, glial activation and neuronal cell loss in the KASE rat model of TLE

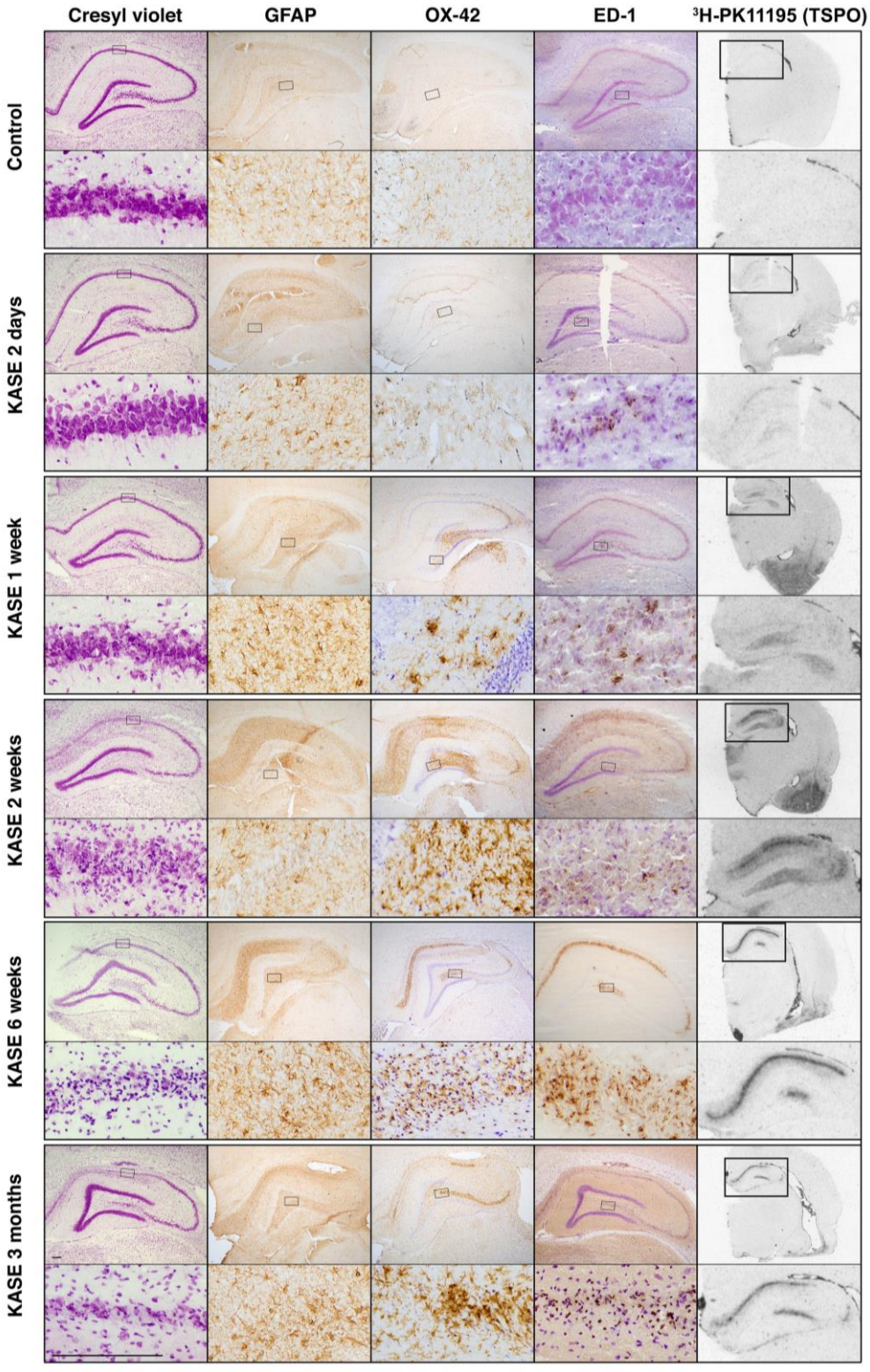

Figure 1. Cell loss, glial activation and TSPO upregulation in the KASE rat model of TLE. Cell loss (cresyl violet), reactive astrocytes (GFAP), activated microglia (OX-42 and ED-1) and TSPO upregulation (^{3}H-PK11195) on coronal brain sections through the hippocampus of representative control and KASE rats. For each time point, sections are shown of the same animal. Brain inflammation and TSPO upregulation is peaking around 2 weeks post-SE and is gradually declining, but remains elevated throughout the chronic epilepsy phase. Inserts are taken in the CA1, CA4 or dentate hilar region. Scale bar= 100 µm. Abbreviations: KASE= kainic acid-induced *status epilepticus*; TSPO= translocator protein.

TSPO expression profile in the brain changes over time

The specific binding of ^{3}H-PK11195 was primarily increased in the temporal lobe, a region known to be involved in epileptic activity, which includes the hippocampus, amygdala, piriform cortex and entorhinal cortex (Figure 1). Consistently, at each time point investigated, significant upregulation of the specific binding was demonstrated in these regions in the KASE group compared to the control group (Figure 2A). The corpus callosum, parietal cortex, thalamus and hypothalamus occasionally showed a significant higher TSPO specific binding in the KASE group (Figure 2A), although not to the extent as the temporal lobe.

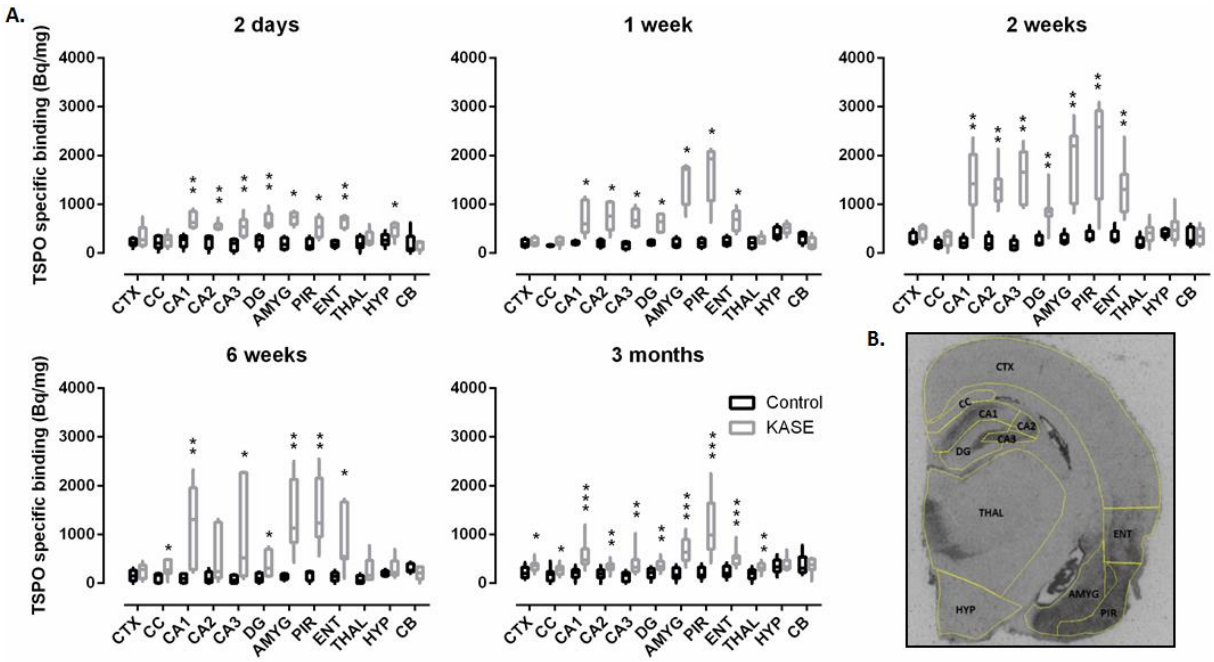

Figure 2. TSPO's spatiotemporal distribution pattern. A. Upregulation of the TSPO specific binding was evident at all time points with highest values 2 and 6 weeks post-insult. **B.** Regions of interest

delineated on a representative KASE animal (2 weeks post-SE) according to the Paxinos and Watson atlas (Paxinos and Watson, 2007). Data are represented as median ± interquartile ranges; *p<0.05, **p<0.01 and ***p<0.001 compared to control; Mann-Whitney U test. Abbreviations: CTX= cortex; CC= corpus callosum; CA= cornu ammonis; DG= dentate gyrus; AMYG= amygdala; PIR= piriform cortex; ENT= entorhinal cortex; THAL= thalamus; HYP= hypothalamus; CB= cerebellum.

When evaluating the temporal expression profile of the TSPO specific binding, it was obvious, especially for the temporal lobe regions that the expression peaked during the latent phase, more specifically 2 weeks post-SE (Figure 2A). Significant differences over time (Kruskal-Wallis test) could be demonstrated for the temporal lobe regions (*p* value ranging from <0.05 to <0.001), the cortex ($p<0.05$) and cerebellum ($p<0.05$). Compared to the time point with the highest expression (2 weeks post-SE), post-hoc tests revealed a significant increase of TSPO expression from 2 days to 2 weeks post-SE for the amygdala ($p<0.05$) and piriform cortex ($p<0.01$), and from 1 week to 2 weeks post-SE for the cortex ($p<0.05$). At the 6 weeks' time point, a significant decrease was found in the hippocampal subregions CA2 ($p<0.01$) and DG ($p<0.01$), and cortex ($p<0.05$). At the 3 months' time point, specific TSPO binding was even more decreased than at 6 weeks post-SE, and compared to 2 weeks post-SE significant decreases could be demonstrated in CA1 ($p<0.05$), CA2 ($p<0.001$), CA3 ($p<0.001$), DG ($p<0.001$), amygdala ($p<0.01$) and entorhinal cortex ($p<0.01$). However, at each time point the TSPO specific binding was still obviously higher in KASE animals compared to control rats.

Interestingly, the increased expression of the TSPO specific binding was most of the time confined to a subarea within the delineated brain region (Figure 2B). The temporal pattern of this focal TSPO binding was different to that of the TSPO specific binding across the whole ROI. As shown in figure 3A, this peaked 6 weeks post-SE in all temporal lobe regions, except for the piriform cortex where the TSPO focal binding reached a peak 2 weeks post-SE. When analysing the temporal evolution of the size of the focal expression of TSPO (TSPO % area), a similar pattern as the TSPO specific binding was demonstrated, with the highest spatial coverage 2 weeks post-SE (Figure 3B).

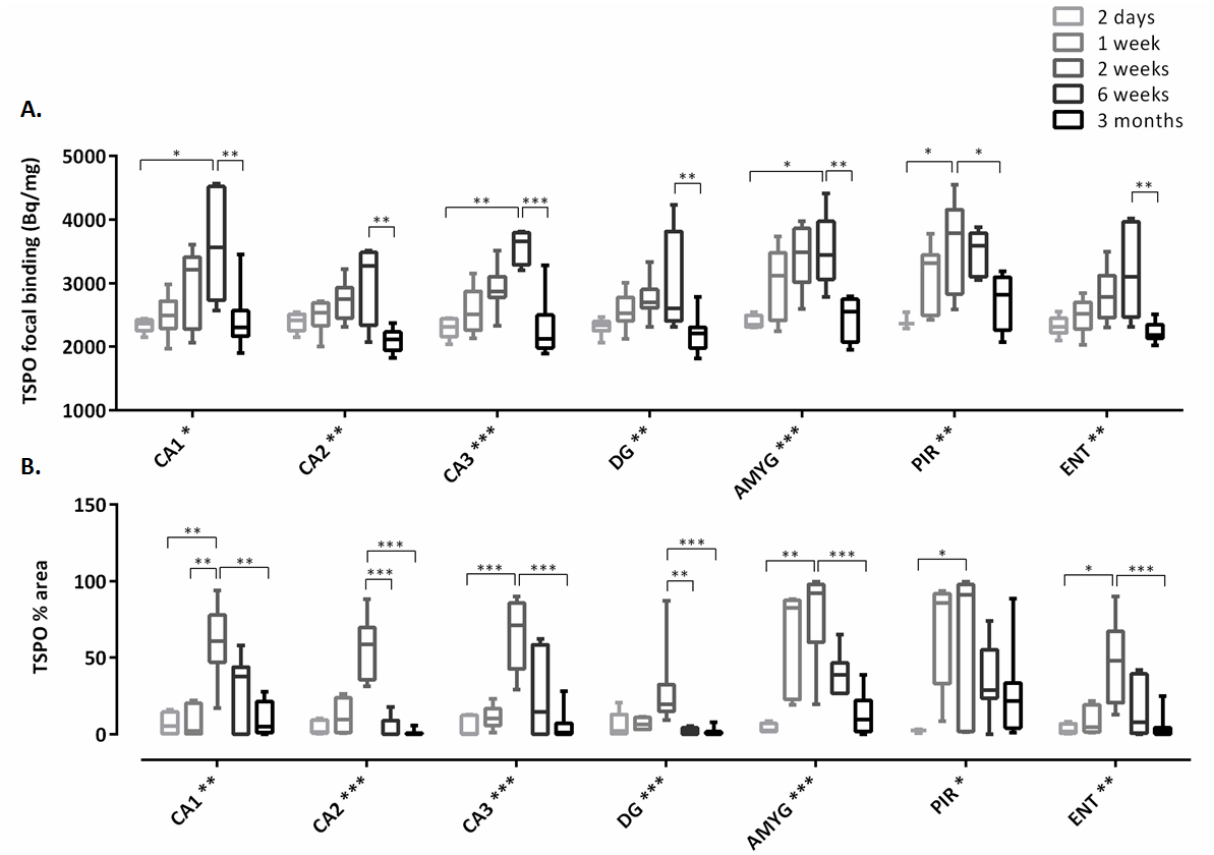

Figure 3. Temporal evolution of the TSPO focal binding and focus size in the temporal lobe regions. **A.** TSPO total binding in the focus area was increasing up to 6 weeks, and again decreasing to 3 months post-SE for all regions, except for the piriform cortex. TSPO focal binding in the piriform cortex peaked 2 weeks post-SE. **B.** Measured focus size of TSPO binding, given as the TSPO % area above the threshold of the whole ROI was increasing up to 2 weeks post-SE, and decreasing to 3 months post-insult. Data are represented as median ± interquartile ranges; *p<0.05, **p<0.01 and ***p<0.001 compared to the peak; Kruskal-Wallis test with Dunn's multiple comparisons test. Abbreviations: CA= cornu ammonis; DG= dentate gyrus; AMYG= amygdala; PIR= piriform cortex; ENT= entorhinal cortex.

Spatiotemporal activation pattern of microglia

By using two different histological markers for the visualisation of microglia (OX-42 and ED-1), our results clearly demonstrate the prominent presence of activated microglia in the KASE model (Figure 1). Similar to TSPO expression, significant increased scores could be demonstrated at all time points, especially in the temporal lobe regions when comparing the KASE to the control group (Figure 4 and 5). The temporal pattern of the ED-1-positive microglia was different from that of OX-42-positive

microglia: while the expression of ED-1 peaked 6 weeks post-SE, which was similar to the TSPO focal binding pattern, OX-42-immunoreactivity peaked 2 weeks post-SE.

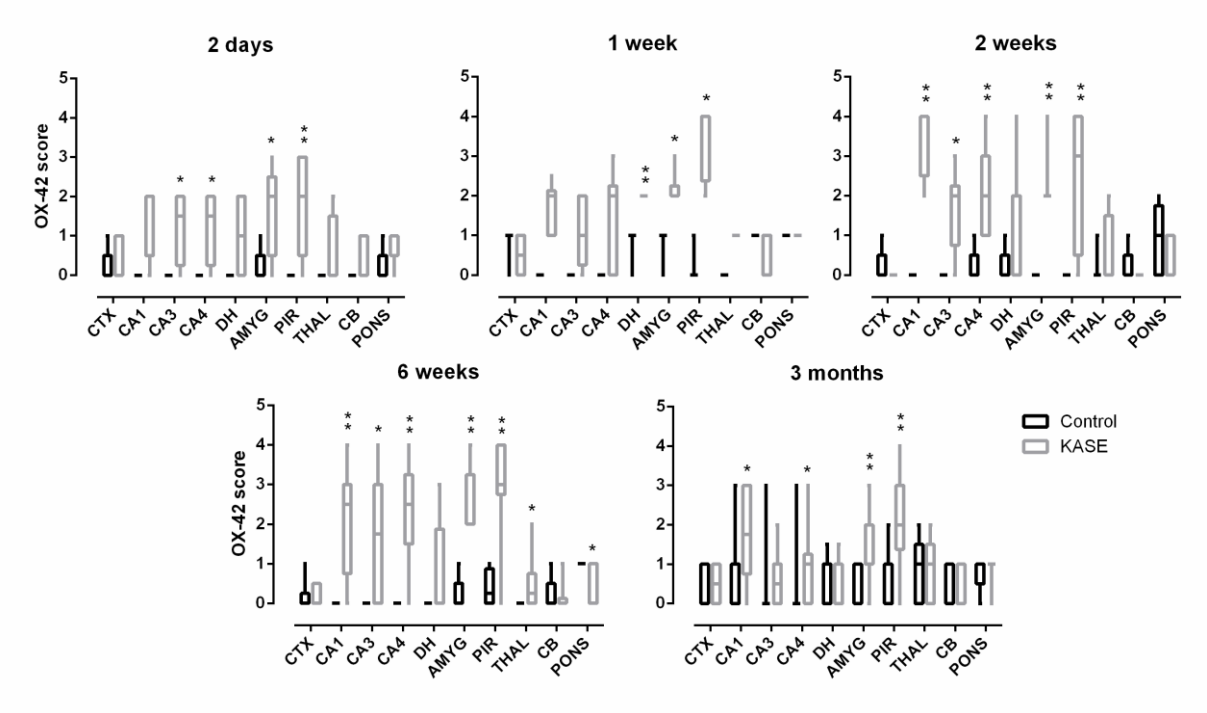

Figure 4. Spatiotemporal distribution of OX-42-positive cells. A significant higher number of OX-42-positive cells was demonstrated at each time point, mainly in the temporal lobe regions. Data are represented as median ± interquartile ranges; *p<0.05, **p<0.01 compared to control; Mann-Whitney U test. Abbreviations: CTX= cortex; CA= cornu ammonis; DH= dentate hilus; AMYG= amygdala; PIR= piriform cortex; THAL= thalamus; CB= cerebellum.

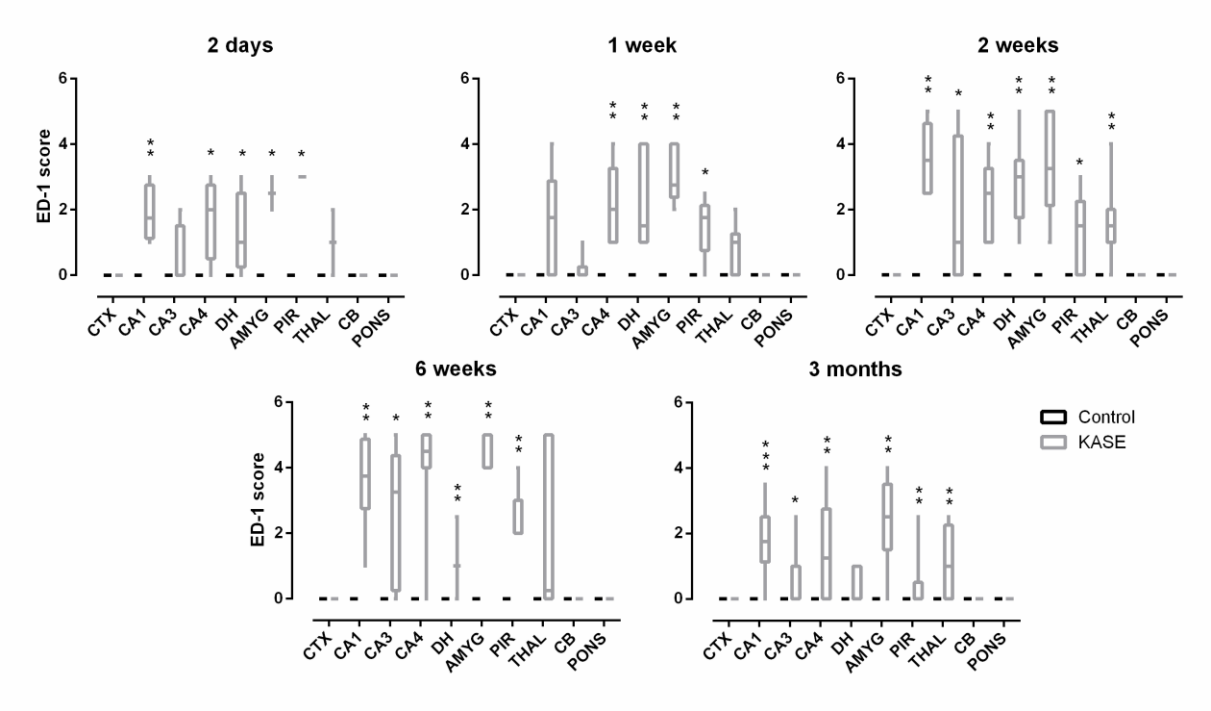

Figure 5. Spatiotemporal distribution of activated microglia (ED-1). Already two days post-insult until the chronic phase, significant differences could be demonstrated between control and KASE animals. Again, the temporal lobe regions are the main regions affected. Data are represented as median ± interquartile ranges; *p<0.05, **p<0.01; ***p<0.001 compared to control; Mann-Whitney U test. Abbreviations: CTX= cortex; CA= cornu ammonis; DH= dentate hilus; AMYG= amygdala; PIR= piriform cortex; THAL= thalamus; CB= cerebellum.

Spatiotemporal activation pattern of astrocytes

The presence of activated astrocytes was evaluated by visualizing GFAP (Figure 1) which showed a more homogenously layered pattern compared to the sometimes focal increases observed for ED-1 or OX-42. For instance, at six weeks the whole CA1 area was covered by reactive astrocytes, while activated microglia (and TSPO) were confined to the pyramidal cell layer (Figure 1). Again, increased GFAP scores compared to control animals were found in the temporal lobe regions of the KASE animals (Figure 6). Importantly, increased GFAP scores were primarily significant 2 and 6 weeks post-SE. Compared to the OX-42 and ED-1 results, fewer regions showed GFAP enhancement at the other time points. When evaluating the temporal evolution of the GFAP enhancement, a consistent pattern was only visible for the hippocampus showing a peak 2 weeks post-SE in all subregions.

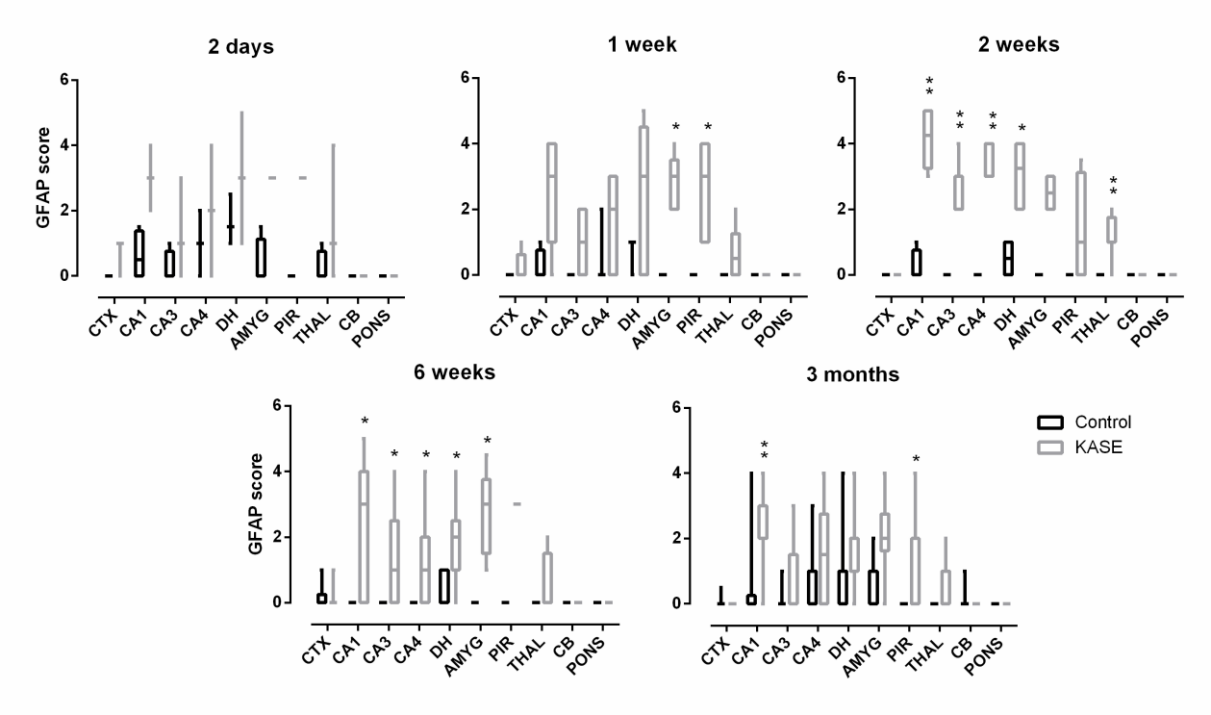

Figure 6. Spatiotemporal distribution pattern of reactive astrocytes. GFAP enhancement was evident especially 2 and 6 weeks post-SE when comparing control with KASE animals. Data are represented as median ± interquartile ranges; *p<0.05, **p<0.01 compared to control; Mann-Whitney U test. Abbreviations: CTX= cortex; CA= cornu ammonis; DH= dentate hilus; AMYG= amygdala; PIR= piriform cortex; THAL= thalamus; CB= cerebellum.

Cell loss in the hippocampus

NeuN staining showed a decrease in cell density in all subregions of the hippocampal formation at all time points (Figure 7). When evaluating the hippocampal neuronal cell loss within the KASE group over time, no significant changes could be demonstrated indicating that the decrease in cell density remained stable over time in the KASE animals.

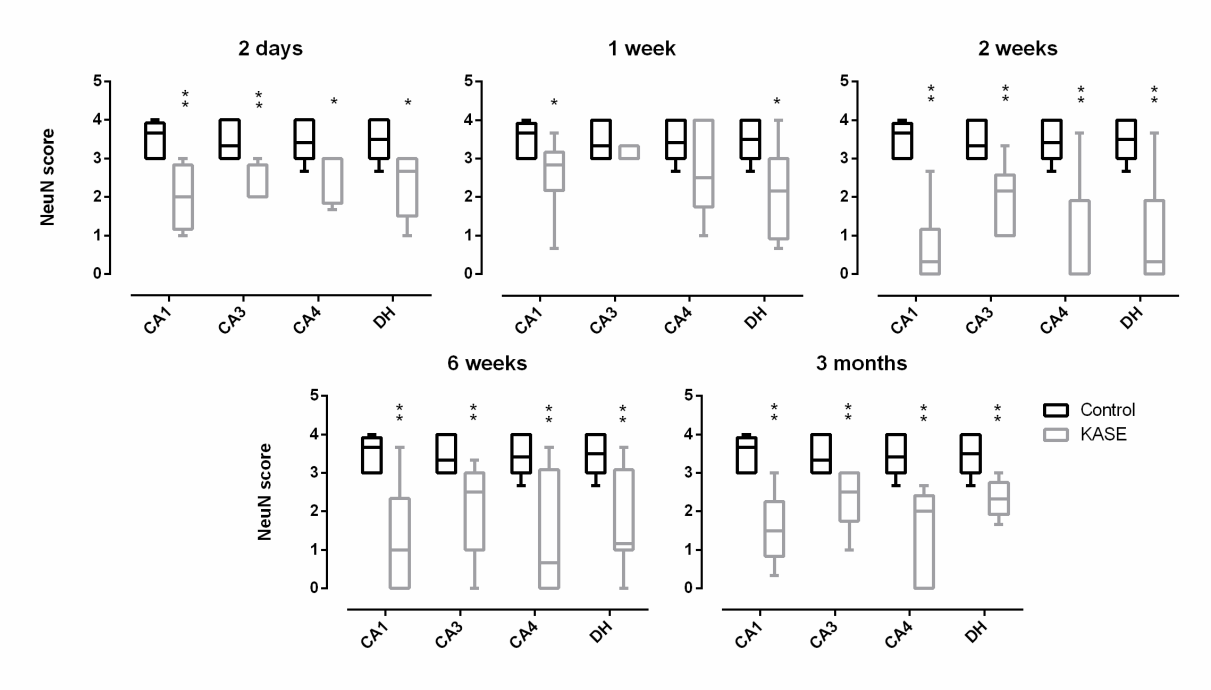

Figure 7. Neuronal cell loss in the hippocampus. Decrease in cell density was present at all time points. A higher NeuN score indicates less neuronal cell loss, while a lower score indicates more cell loss. There was no variability between the control animals over the different time points and therefore, they were pooled together for comparison with the different KASE groups. Data are represented as median ± interquartile ranges; *p<0.05, **p<0.01, ***p<0.001 compared to control; Mann-Whitney U test. Abbreviations: CA= cornu ammonis; DH= dentate hilus.

TSPO upregulation reflects microglial activation and neurodegeneration

Visually, the regional expression profile of TSPO broadly corresponded to the spatial pattern of OX-42- and ED-1-immunoreactivity (Figure 1). Relating the OX-42 score of all KASE animals across time with the different TSPO variables (TSPO specific binding, TSPO focal binding and TSPO % area) for the hippocampus resulted in significant positive correlations (p<0.001 and r=0.6; p<0.01 and r=0.6, and p<0.01 and r=0.5 respectively). Moreover, when correlating the ED-1 score with these variables, even stronger and significant positive correlations were seen (p<0.001; r=0.8, r=0.7 and r=0.8 respectively). When associating astrocyte reactivity with these variables, significant positive, but weak correlations could only be demonstrated for the TSPO specific binding (p<0.01 and r=0.5) and TSPO % area (p<0.01 and r=0.6). In parallel to microglial activation, the NeuN score also strongly

related to all three variables for the hippocampus (p<0.001 and r=-0.7; p<0.001 and r=-0.8, and p<0.001 and r=-0.7 respectively). In figure 8, the correlation between the TSPO focal binding and the different histological markers is shown.

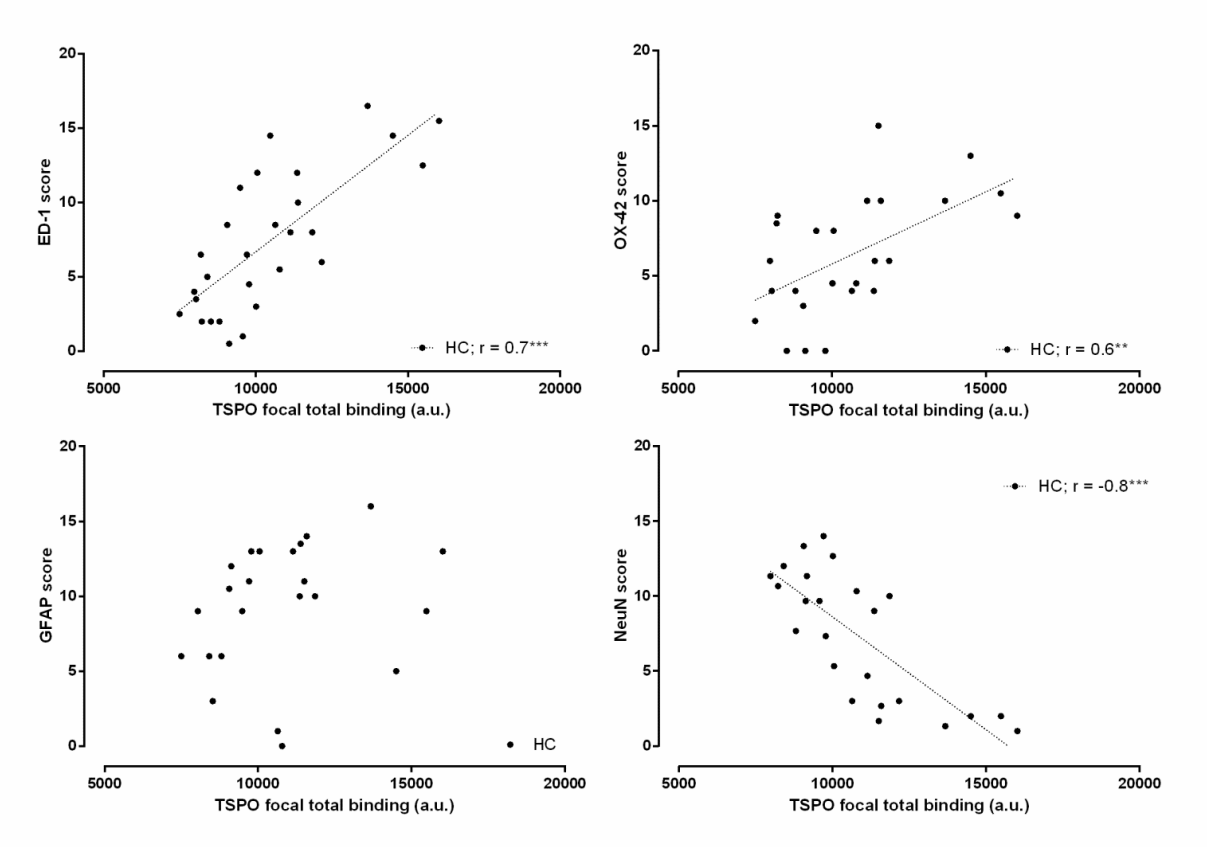

Figure 8. TSPO upregulation reflects microglial activation and is positively correlated with cell loss. The graphs represent the relationship between TSPO focal total binding and the ED-1, OX-42, GFAP and NeuN score respectively, in the hippocampus. Microglial activation, especially the ED-1-positive cell population significantly correlates with TSPO which is in contrast to astrocyte reactivity. A relationship between the reduction of hippocampal cell loss and TSPO focal total binding could also be demonstrated. *p<0.05, **p<0.01 and ***p<0.001; Spearman's rank correlation test. Abbreviations: HC= hippocampus.

Evaluation of spontaneous recurrent seizures: positive relationship between seizures and TSPO binding

During the transition phase (6 weeks post-SE), only two out of the 10 KASE animals experienced SRS (0.24 and 0.48 per day). In contrast, during the chronic phase (3 months post-SE), 9 out of 12 (75%)

animals experienced seizures. The number of SRS ranged between 0 to 1.68 per day (0.64 ± 0.15 SRS per day). Control animals did not experience any seizures. According to the scale of Racine, the two animals of the 6 weeks' time point experienced type 4 seizures, while the chronic epileptic animals displayed seizures covering the entire scale. However, the large majority of the observed seizures were convulsive seizures (29 out of 32).

The relationship between the number of SRS per day and the TSPO specific binding was studied to assess whether TSPO expression in the chronic period is associated with the epilepsy outcome. Significant positive correlations (Spearman's rank) could be shown for the DG ($p< 0.01$ and r= 0.6), entorhinal cortex ($p< 0.05$ and r= 0.5), piriform cortex ($p< 0.05$ and r= 0.7), thalamus ($p< 0.01$ and r= 0.6) and parietal cortex ($p< 0.01$ and r= 0.6) (Figure 9). Thus showing a higher TSPO expression in several regions in the KASE animals that experienced more SRS per day.

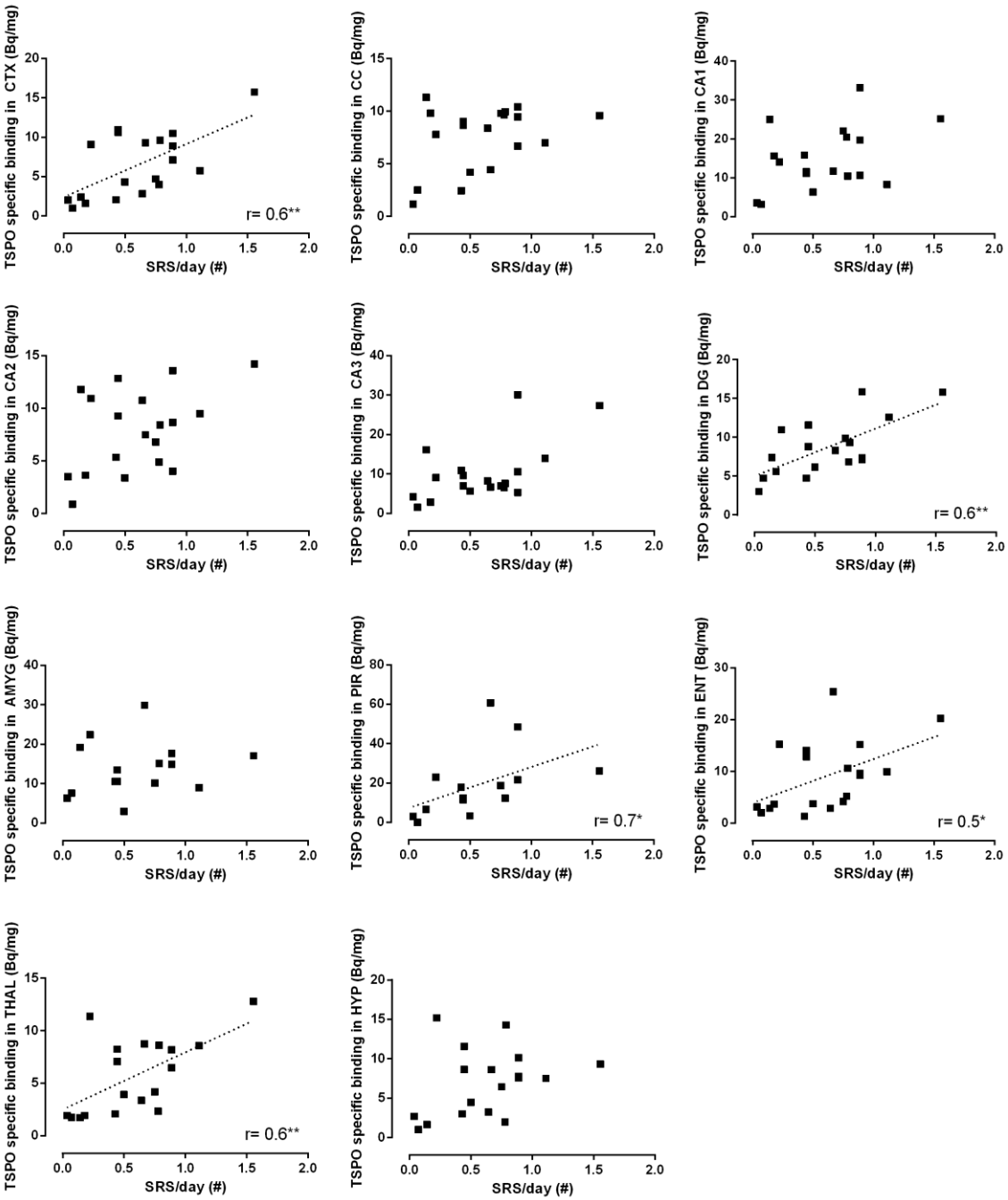

Figure 9. Relationship between SRS and TSPO in chronic epilepsy rats. A positive and significant relationship could be established between the number of SRS per day and the TSPO specific binding for the DG, entorhinal and piriform cortices, thalamus and (parietal) cortex within the KASE group. **p*< 0.05, ***p*<0.01; Spearman's rank correlation test. Abbreviations: CTX= cortex, CA= cornu ammonis; DG= dentate gyrus; AMYG= amygdala; PIR= piriform cortex; ENT= entorhinal cortex; THAL= thalamus; HYP= hypothalamus.

Successful *in vivo* longitudinal follow-up of TSPO expression

Due to the advantage of 3-D visualisation of TSPO binding in the whole brain with PET (compared to sectional histology), it was seen that TSPO increases extended across the whole limbic system. The *in vivo* follow-up of TSPO expression in the brain by means of consecutive ^{18}F-PBR111 PET scans, executed 2 and 4 (for four animals), and also at 6 weeks (for two out of the four animals) post-SE showed high ^{18}F-PBR111 binding 2 weeks post-SE in the limbic system, which declined over time (Figure 10). At 4 weeks post-SE a decrease of about 15 to 30% was seen in the different limbic regions. We could still visualise TSPO overexpression in those regions 6 weeks after induction of the SE (Figure 10 and Supplementary video 1, see online). However a decrease of about 40 to 50% was noted compared to 2 weeks post-insult. The MRI scans, which were taken in parallel, showed volumetric increase of the ventricles and hippocampal shrinkage in some animals. The volumetric changes of the ventricles were ongoing during the latent (2 weeks post-insult) and transition phase (4 and 6 weeks post-SE) in one out of the four animals. Hippocampal shrinkage was visible in two out of the four animals from 2 weeks post-SE to 4 weeks post-insult. The decrease in hippocampal volume in the two animals that were additionally scanned 6 weeks post-SE seemed to be ceased at that time point.

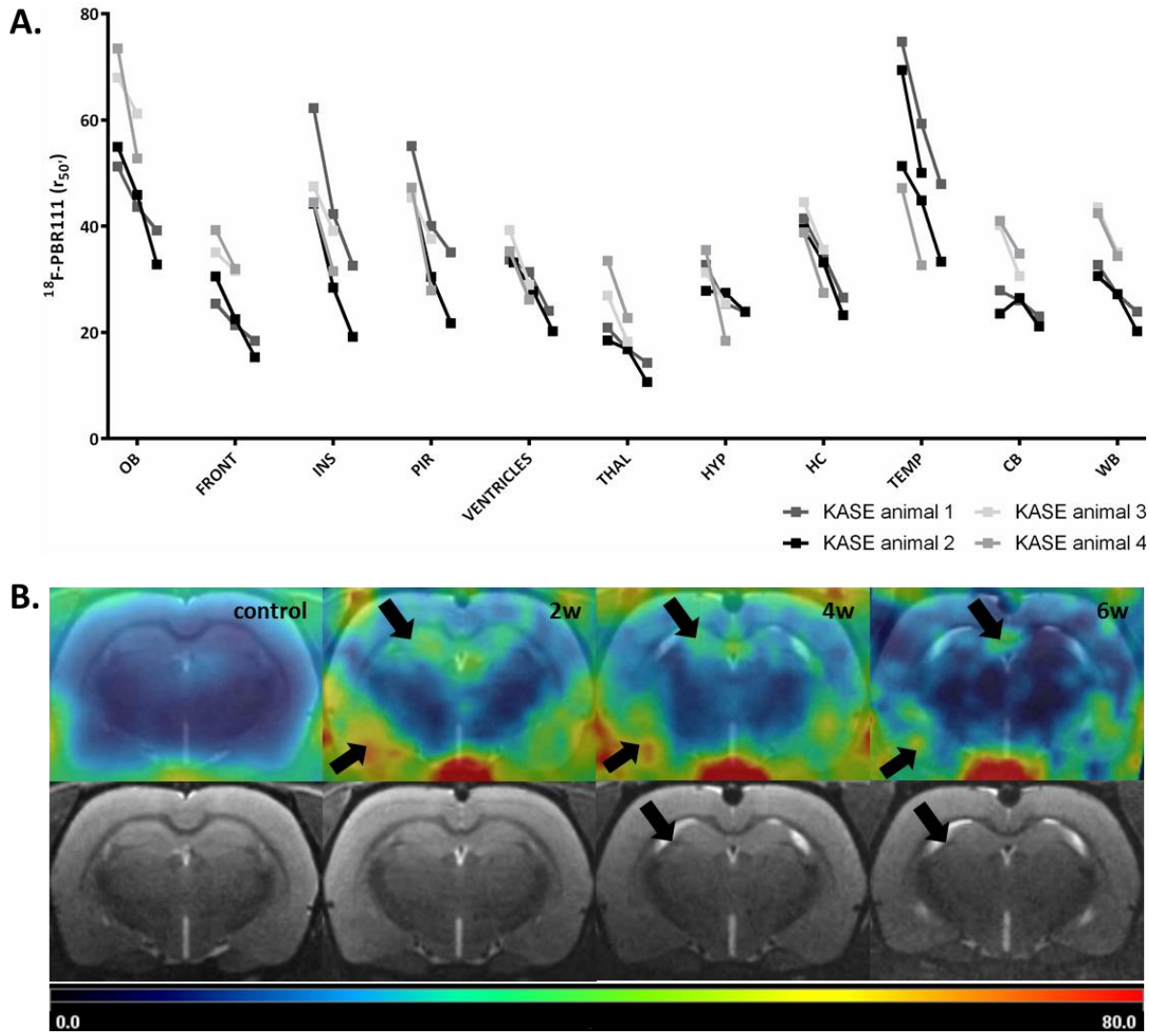

Figure 10. Longitudinal follow-up of TSPO binding in the KASE model of TLE. A. The 2-week ^{18}F-PBR111 PET scan showed high levels of TSPO binding *in vivo*. Longitudinal PET scans consistently demonstrated a decrease in ^{18}F-PBR111 tracer binding in all regions investigated at 4 weeks post-insult when compared to 2 weeks post-SE for all four KASE animals. The same was applicable when comparing 6 weeks to 2 weeks post-insult for the two KASE animals scanned 6 weeks post-SE. **B.** ^{18}F-PBR111 PET image (50' ratio) and corresponding MRI of a control animal 2 weeks post-insult and a KASE rat taken 2, 4 and 6 weeks post-SE. The decrease of TSPO binding was clearly visible over time in the temporal lobe regions (arrows) shown on the PET images, while ventricular enlargement and hippocampal shrinkage was visible on the MRI images (arrows). Abbreviations: OB= olfactory bulbus; FRONT= frontal cortex; INS= insular cortex; PIR= piriform network; THAL= thalamus; HYP= hypothalamus; HC= hippocampus; TEMP= temporal cortex; CB= cerebellum; WB= whole brain.

Supplementary video 1 (see online doi: 10.1016/j.nbd.2015.09.004.). 3-D visualisation of the spatiotemporal distribution of the TSPO PET 50' ratio. The three videos belong to the same animal but to different time points post-SE, namely 2, 4 and 6 weeks post-SE. The initial high increases in TSPO binding in the limbic regions were substantially decreasing, but still detectable towards 6 weeks post-SE.

Discussion

To summarize, our results suggest that TSPO upregulation is associated with activated microglia rather than reactive astrocytes during epileptogenesis and established epilepsy in the temporal lobe regions of KASE animals. A decrease in neuronal cell density was visible in the hippocampus at each time point and was associated with increased TSPO levels. Importantly, a positive relationship between the number of SRS per day and the TSPO binding was also shown in the chronic epilepsy phase. Finally, longitudinal non-invasive PET measurements allowed identifying the evolution of TSPO binding within brain networks in the same subject over time which was confirmed by the *post-mortem* results.

A regional distribution of TSPO upregulation was evident, i.e. the hippocampus, amygdala, piriform cortex and entorhinal cortex were the main regions showing increased expression in contrast to the parietal cortex, hypothalamus and cerebellum. This was expected because the temporal lobe regions are known to be susceptible to the development of seizures (Kelly and McIntyre, 1996; Ebert et al., 2000; Wittner et al., 2005). The PET studies showed that the increase in temporal lobe regions encompasses the whole limbic system. This is in accordance to our previous results (Dedeurwaerdere et al., 2012a) and the findings of other research groups (Altar and Baudry, 1990; Johnson et al., 1992; Kumlien et al., 1992).

When evaluating the temporal pattern of TSPO expression, our findings indicate an overall upregulation during the early, latent and chronic phase. Highest TSPO expression was seen 2 weeks post-SE, which declined, but remained high 6 weeks after the insult in the temporal lobe regions. In accordance, preceding animal studies have demonstrated enhanced TSPO levels up to 6 weeks after an epileptogenic insult (Altar and Baudry, 1990; Guilarte et al., 1995). The current findings extend beyond this point and show persistent TSPO upregulation 3 months post-SE (established epilepsy). This is in agreement with studies in patients with TLE, represented by the chronic phase in the KASE model. Studies on post-surgical human tissue found increased TSPO expression in specific regions

important for seizure generation (Johnson et al., 1992; Kumlien et al., 1992; Sauvageau et al., 2002). To further investigate the evolution of TSPO expression, we also analysed the focal binding and the percentage area of the focal expression. A difference was demonstrated for the focal binding as this peaked 6 weeks instead of 2 weeks post-SE when compared to the TSPO % area and the TSPO specific binding. Thus the upregulation of TSPO was most intense during the transition phase, while the TSPO % area of the focal expression and, in parallel, the TSPO specific binding peaked earlier during epileptogenesis (latent phase). This might imply that during the latent phase when the normal brain is undergoing several different changes, TSPO is more widely expressed within the brain regions important for seizure generation. However, during the transition phase when the probability for the occurrence of SRS is much higher and the normal brain has changed more or less to an epileptic one, TSPO is really confined to much smaller areas. This could be relevant when determining the therapeutic window for manipulating TSPO expression.

In a previous study, we suggested that TSPO upregulation is confined to areas with higher levels of microglia activation (OX-42) in the KASE model (Dedeurwaerdere et al., 2012a). However, we did not look at the association with other microglia markers, such as ED-1, or with astrocytes. Overall, microglial activation as well as astrocyte reactivity were increased during the latent and transition phase and decreased towards the chronic phase, which was in accordance with studies executed before (Hattiangady et al., 2004; Ravizza et al., 2008; Sharma et al., 2008; Drexel et al., 2012). An important contribution of this study was the investigation of the association between TSPO expression and glial cells. The spatial expression of the microglial markers OX-42 and ED-1 resembled the pattern of TSPO enhancement (Figure 1) during the different phases of epileptogenesis in different brain regions. More specifically, a consistent and strong positive correlation was found between TSPO expression and ED-1-immunoreactivity in the hippocampus. Indeed, other animal models of brain damage have shown that microglia can be the cellular source of TSPO expression by co-localization of microglial markers and TSPO with immunofluorescence double labelling (Ji et al., 2008; Cosenza-Nashat et al., 2009; Martin et al., 2010). Importantly, recent studies also have shown

astrocytes to increase TSPO expression when activated (Cosenza-Nashat et al., 2009; Lavisse et al., 2012). However, Ji et al. (2008) revealed microglia, in contrast to astrocytes, to colocalise with TSPO in the KASE model (1 week post-SE) herein using an in-house developed NP155 antibody for TSPO. Our data showed that the association was much stronger with ED-1 than with OX-42, which suggests that TSPO upregulation might be even more related to the activated, phagocytic microglia population. However, this has to be confirmed by a colocalisation study which was unfortunately not performed due to the absence of a well-performing commercial available TSPO antibody for rat.

Our study showed a prominent association between decreased neuronal cell density and the TSPO levels in the hippocampus. Altar and Baudry (1990) proposed that early TSPO upregulation in the KASE model serves as an inherent glial response to neuronal loss. In a rat model of excitotoxicity and Parkinson's disease, it was demonstrated that brain inflammation and neurodegeneration, assessed by visualisation of TSPO, occurred concomitantly over time (Maia et al., 2012; Arlicot et al., 2014). These studies support the association between cell loss and TSPO and thus our observation. We believe that this relationship reflects the association of brain inflammation in general, for example microglial activation, and cell loss. Cell loss results in cell debris which is cleared by activated and phagocytic microglia that upregulate TSPO expression. Likewise, different studies showed a link between neuronal loss and microglial cells in the CA1 and CA3 hippocampal subregions (Sharma et al., 2008; Zattoni et al., 2011). When interpreting the relationship between TSPO expression and cell loss in the context of the chronic period, it is important to note that our findings indicated that the decrease in neuronal cell density seen in the KASE animals stayed stable over time in the hippocampus. This means that probably the cell loss is resulting from cell damage during the early phases. However, Pitkänen and colleagues identified degenerating hippocampal neurons up to 68 days post-SE, indicating that some degree of neurodegeneration can still be ongoing past early epileptogenesis (Pitkanen et al., 2002). Therefore, it is conceivable that, although in lower numbers, immune-competent cells expressing TSPO may still be clearing degenerating cells at that time point.

Our results show persistent upregulation of TSPO, microglia activation and reactive astrocytes throughout the chronic phase when the rats have established epilepsy and thus experience SRS. This insinuates a potential relationship between chronic inflammation and disease outcome. Indeed, previously it has been shown that brain inflammation can cause hyperexcitability through the production of certain cytokines, e.g. TNF-α and IL-1β (Hu et al., 2000; Dube et al., 2005; Stellwagen et al., 2005; Galic et al., 2012). In addition, a positive correlation was found between brain inflammation and seizures (Boer et al., 2006; Ravizza et al., 2006). Thus, while the early and widespread TSPO upregulation is likely to be induced by the initial injury, i.e. SE, the persistent presence up to the point of chronic TLE suggests potential involvement of TSPO in transition to the epileptic state. In accordance, this study showed positive correlations between the number of seizures during the chronic period with the *post-mortem* TSPO binding in limbic regions, but also beyond (thalamus and parietal cortex). Also a previous study indicated that *in vivo* TSPO binding might reflect seizure frequency in a SE model (Bogdanovic et al., 2014). However, they could not demonstrate this relationship when only taking the 20 – 60 min time frame into account, which is considered to more reliably represent the specific binding of the tracer (Bogdanovic et al., 2014; Dickens et al., 2014). Chen et al. (2008) showed higher TSPO densities to be related with increased seizure intensity and decreased seizure latency in KA-kindled rats. The role of TSPO in epileptogenesis is still unsure. TSPO is involved in divergent mechanisms and has been associated with protective homeostatic mechanisms, such as in neurosteroid synthesis. This could preserve the rats from having seizures (Biagini et al., 2006). On the other hand, TSPO is involved in apoptosis and may also support microglia proliferation, which could lead to negative consequences of TSPO upregulation.

A major advantage of TSPO is that it can be measured *in vivo* by PET, which is important when translating to the clinic. PET imaging of TSPO has already been translated to the clinic on a small scale. Case reports using *in vivo* TSPO PET imaging for determination of the underlying pathology or to identify the epileptogenic zone have been published (Banati et al., 1999; Goerres et al., 2001; Kumar et al., 2008; Butler et al., 2013). In a study of Hirvonen et al. (2012) with 16 TLE patients, an

increased uptake of ^{11}C-PBR028, another TSPO PET ligand, was shown ipsilateral to the seizure focus. Accordingly, a recent study in patients with TLE of Gershen et al. (2015) showed increased TSPO binding ipsilateral and contralateral to the seizure focus in the temporal lobe regions by ^{18}F-PBR028 and ^{11}C-DPA713. The non-invasiveness of PET makes it also attractive to follow-up a test subject longitudinally. To demonstrate this, we assessed the temporal and spatial evolution of TSPO in KASE animals by means of ^{18}F-PBR111 PET. The dynamic nature of TSPO upregulation during epileptogenesis in our cross-sectional histology study was visualised within the same animal with the PET study. All regions that showed high tracer uptake in early stages, still showed elevated levels of ^{18}F-PBR111 binding 4 and 6 weeks after induction of the SE as compared to control, but this was attenuated as compared to the 2 weeks' time point. Thus, both the cross-sectional and the longitudinal PET study revealed the same results for the temporal expression of TSPO. This signifies that *in vivo* PET imaging with ^{18}F-PBR111 is a valid method to follow-up TSPO expression over time in the same subject. The dynamic temporal pattern of TSPO binding is reflected by the TSPO specific binding measurement rather than the focal binding on autoradiography. This can be attributed to the partial volume effect, typical for PET imaging (lower resolution compared to autoradiography). Importantly PET allows investigating 3-D changes in TSPO binding and our PET data revealed that also other regions than the regions investigated with autoradiography had a high TSPO expression.

TSPO PET imaging could be a powerful tool in identifying network dysfunctions in prospective studies. New studies can now investigate whether the huge increases in TSPO after brain insult are related to the epilepsy outcome. Potentially, these network alterations after an initial insult may help stratifying subjects before epilepsy diagnosis. Altogether, this raises the possibility to follow up patients at risk over time and to evaluate *in vivo* new therapies which manipulate TSPO expression.

To conclude, we demonstrated that TSPO upregulation follows the same spatiotemporal pattern as that of activated microglia in the KASE model. It peaks during the latent period and persists throughout the chronic period when animals have developed epilepsy. In addition, this biomarker for

brain inflammation was shown to be associated with the number of seizures during the chronic period. Finally, we successfully followed up the evolution of this biomarker *in vivo* over time using ^{18}F-PBR111 PET. Follow-up studies are necessary to further unravel the complex relationship between TSPO expression and epilepsy outcome, and the role of TSPO in epileptogenesis. This will teach us whether TSPO is a potential candidate for the development of novel treatment strategies and a potential biomarker for predicting epilepsy outcome.

Acknowledgements

First of all, we would like to thank MICA, especially J Parthoens and P Joye, for their consistent assistance, especially at the start of our experiments. We would also like to thank I Bats for her excellent work in compiling figure 1. Our gratitude also goes to E Jonckers and J Goossens for their assistance in the imaging part. Finally, we also want to thank our lab technicians K Szewczyk and A Van Eetveldt for their great support. Stefanie Dedeurwaerdere is supported by the Research Foundation Flanders (FWO) funding 1.5.110.14N, 1.5.144.12N and ERA-NET NEURON G.A009.13N, and finally by the Queen Elisabeth Medical Foundation (Q.E.M.F.) for Neurosciences. Halima Amhaoul, Stefanie Dedeurwaerdere and Steven Staelens are supported by the Bijzonder Onderzoeks Fonds (BOF) of the University of Antwerp. Annemie Van Der Linden is supported by the European Union's Seventh Framework Programme under grant agreement number 278850 (INMiND). The Laboratory of Neurochemistry and Behaviour is supported by the Research Foundation-Flanders (FWO), Interuniversity Poles of Attraction (IAP Network P7/16) of the Belgian Federal Science Policy Office, Methusalem excellence grant of the Flemish Government, agreement between Institute Born-Bunge and University of Antwerp, the Medical Research Foundation Antwerp, the Thomas Riellaerts research fund, and Neurosearch Antwerp.

Authors contributions

For this manuscript all authors contributed profoundly to the manuscript: *study concept and design:* Halima Amhaoul, Steven Staelens and Stefanie Dedeurwaerdere; *PET tracer validation and synthesis:*

Halima Amhaoul, Jeroen Verhaeghe, Andrew Katsifis, Steven Staelens and Stefanie Dedeurwaerdere; *data acquisition:* Halima Amhaoul, Daniele Bertoglio, Jeroen Verhaeghe, Elly Geerts, Debby Van Dam, Peter Paul De Deyn, Annemie Van Der Linden, Steven Staelens and Stefanie Dedeurwaerdere; *data quantification:* Halima Amhaoul, Julie Hamaide, Stephanie Nadine Reichel and Stefanie Dedeurwaerdere; *data analysis and interpretation:* Halima Amhaoul, Julie Hamaide, Stephanie Nadine Reichel, Jeroen Verhaeghe, Samir Kumar-Singh, Steven Staelens and Stefanie Dedeurwaerdere; *writing of the manuscript:* Halima Amhaoul, Julie Hamaide, Steven Staelens and Stefanie Dedeurwaerdere; *critically editing and revising the manuscript:* Halima Amhaoul, Julie Hamaide, Stephanie Nadine Reichel, Daniele Bertoglio, Jeroen Verhaeghe, Elly Geerts, Debby Van Dam, Peter Paul De Deyn, Samir Kumar-Singh, Andrew Katsifis, Annemie Van Der Linden, Steven Staelens and Stefanie Dedeurwaerdere. None of the authors has any conflict of interest to disclose.

References

Altar CA, Baudry M (1990), Systemic injection of kainic acid: gliosis in olfactory and limbic brain regions quantified with [3H]PK 11195 binding autoradiography. Experimental neurology 109:333-341.

Amhaoul H, Staelens S, Dedeurwaerdere S (2014), Imaging brain inflammation in epilepsy. Neuroscience 279C:238-252.

Arlicot N, Tronel C, Bodard S, Garreau L, de la Crompe B, Vandevelde I, Guilloteau D, Antier D, Chalon S (2014), Translocator protein (18 kDa) mapping with [125I]-CLINDE in the quinolinic acid rat model of excitotoxicity: a longitudinal comparison with microglial activation, astrogliosis, and neuronal death. Molecular imaging 13:4-11.

Banati RB, Goerres GW, Myers R, Gunn RN, Turkheimer FE, Kreutzberg GW, Brooks DJ, Jones T, Duncan JS (1999), [11C](R)-PK11195 positron emission tomography imaging of activated microglia in vivo in Rasmussen's encephalitis. Neurology 53:2199-2203.

Biagini G, Baldelli E, Longo D, Pradelli L, Zini I, Rogawski MA, Avoli M (2006), Endogenous neurosteroids modulate epileptogenesis in a model of temporal lobe epilepsy. Experimental neurology 201:519-524.

Boer K, Spliet WG, van Rijen PC, Redeker S, Troost D, Aronica E (2006), Evidence of activated microglia in focal cortical dysplasia. Journal of neuroimmunology 173:188-195.

Bogdanovic RM, Syvanen S, Michler C, Russmann V, Eriksson J, Windhorst AD, Lammertsma AA, de Lange EC, Voskuyl RA, Potschka H (2014), (R)-[C]PK11195 brain uptake as a biomarker of inflammation and antiepileptic drug resistance: Evaluation in a rat epilepsy model. Neuropharmacology 85C:104-112.

Butler T, Ichise M, Teich AF, Gerard E, Osborne J, French J, Devinsky O, Kuzniecky R, Gilliam F, Pervez F, Provenzano F, Goldsmith S, Vallabhajosula S, Stern E, Silbersweig D (2013), Imaging inflammation in a patient with epilepsy due to focal cortical dysplasia. Journal of neuroimaging : official journal of the American Society of Neuroimaging 23:129-131.

Chen C, Lang S, Xu G, Liu X, Zuo P (2008), Effects of topiramate on seizure susceptibility in kainate-kindled rats: involvement of peripheral-type benzodiazepine receptors. Seizure : the journal of the British Epilepsy Association 17:358-363.

Cosenza-Nashat M, Zhao ML, Suh HS, Morgan J, Natividad R, Morgello S, Lee SC (2009), Expression of the translocator protein of 18 kDa by microglia, macrophages and astrocytes based on immunohistochemical localization in abnormal human brain. Neuropathology and applied neurobiology 35:306-328.

Dedeurwaerdere S, Callaghan PD, Pham T, Rahardjo GL, Amhaoul H, Berghofer P, Quinlivan M, Mattner F, Loc'h C, Katsifis A, Gregoire MC (2012a), PET imaging of brain inflammation during early epileptogenesis in a rat model of temporal lobe epilepsy. EJNMMI research 2:60.

Dedeurwaerdere S, Fang K, Chow M, Shen YT, Noordman I, van Raay L, Faggian N, Porritt M, Egan GF, O'Brien TJ (2013), Manganese-enhanced MRI reflects seizure outcome in a model for mesial temporal lobe epilepsy. NeuroImage 68:30-38.

Dedeurwaerdere S, Friedman A, Fabene PF, Mazarati A, Murashima YL, Vezzani A, Baram TZ (2012b), Finding a better drug for epilepsy: antiinflammatory targets. Epilepsia 53:1113-1118.

Dedeurwaerdere S, van Raay L, Morris MJ, Reed RC, Hogan RE, O'Brien TJ (2011), Fluctuating and constant valproate administration gives equivalent seizure control in rats with genetic and acquired epilepsy. Seizure : the journal of the British Epilepsy Association 20:72-79.

Defrise M, Kinahan PE, Townsend DW, Michel C, Sibomana M, Newport DF (1997), Exact and approximate rebinning algorithms for 3-D PET data. IEEE transactions on medical imaging 16:145-158.

Dickens AM, Vainio S, Marjamaki P, Johansson J, Lehtiniemi P, Rokka J, Rinne J, Solin O, Haaparanta-Solin M, Jones PA, Trigg W, Anthony DC, Airas L (2014), Detection of microglial activation in an acute model of neuroinflammation using PET and radiotracers 11C-(R)-PK11195 and 18F-

GE-180. Journal of nuclear medicine : official publication, Society of Nuclear Medicine 55:466-472.

Drexel M, Preidt AP, Sperk G (2012), Sequel of spontaneous seizures after kainic acid-induced status epilepticus and associated neuropathological changes in the subiculum and entorhinal cortex. Neuropharmacology 63:806-817.

Dube C, Vezzani A, Behrens M, Bartfai T, Baram TZ (2005), Interleukin-1beta contributes to the generation of experimental febrile seizures. Annals of neurology 57:152-155.

Ebert U, Wlaz P, Loscher W (2000), High susceptibility of the anterior and posterior piriform cortex to induction of convulsions by bicuculline. The European journal of neuroscience 12:4195-4205.

Friedman A, Kaufer D, Heinemann U (2009), Blood-brain barrier breakdown-inducing astrocytic transformation: novel targets for the prevention of epilepsy. Epilepsy research 85:142-149.

Galic MA, Riazi K, Pittman QJ (2012), Cytokines and brain excitability. Frontiers in neuroendocrinology 33:116-125.

Gershen LD, Zanotti-Fregonara P, Dustin IH, Liow JS, Hirvonen J, Kreisl WC, Jenko KJ, Inati SK, Fujita M, Morse CL, Brouwer C, Hong JS, Pike VW, Zoghbi SS, Innis RB, Theodore WH (2015), Neuroinflammation in Temporal Lobe Epilepsy Measured Using Positron Emission Tomographic Imaging of Translocator Protein. JAMA neurology 72:882-888.

Goerres GW, Revesz T, Duncan J, Banati RB (2001), Imaging cerebral vasculitis in refractory epilepsy using [(11)C](R)-PK11195 positron emission tomography. AJR American journal of roentgenology 176:1016-1018.

Guilarte TR, Kuhlmann AC, O'Callaghan JP, Miceli RC (1995), Enhanced expression of peripheral benzodiazepine receptors in trimethyltin-exposed rat brain: a biomarker of neurotoxicity. Neurotoxicology 16:441-450.

Hattiangady B, Rao MS, Shetty AK (2004), Chronic temporal lobe epilepsy is associated with severely declined dentate neurogenesis in the adult hippocampus. Neurobiology of disease 17:473-490.

Hirvonen J, Kreisl WC, Fujita M, Dustin I, Khan O, Appel S, Zhang Y, Morse C, Pike VW, Innis RB, Theodore WH (2012), Increased in vivo expression of an inflammatory marker in temporal lobe epilepsy. Journal of nuclear medicine : official publication, Society of Nuclear Medicine 53:234-240.

Hu S, Sheng WS, Ehrlich LC, Peterson PK, Chao CC (2000), Cytokine effects on glutamate uptake by human astrocytes. Neuroimmunomodulation 7:153-159.

Hudson HM, Larkin RS (1994), Accelerated image reconstruction using ordered subsets of projection data. IEEE transactions on medical imaging 13:601-609.

Ji B, Maeda J, Sawada M, Ono M, Okauchi T, Inaji M, Zhang MR, Suzuki K, Ando K, Staufenbiel M, Trojanowski JQ, Lee VM, Higuchi M, Suhara T (2008), Imaging of peripheral benzodiazepine receptor expression as biomarkers of detrimental versus beneficial glial responses in mouse models of Alzheimer's and other CNS pathologies. The Journal of neuroscience : the official journal of the Society for Neuroscience 28:12255-12267.

Johnson EW, de Lanerolle NC, Kim JH, Sundaresan S, Spencer DD, Mattson RH, Zoghbi SS, Baldwin RM, Hoffer PB, Seibyl JP, et al. (1992), "Central" and "peripheral" benzodiazepine receptors: opposite changes in human epileptogenic tissue. Neurology 42:811-815.

Katsifis A, Loc'h C, Henderson D, Bourdier T, Pham T, Greguric I, Lam P, Callaghan P, Mattner F, Eberl S, Fulham M (2011), A rapid solid-phase extraction method for measurement of non-metabolised peripheral benzodiazepine receptor ligands, [(18)F]PBR102 and [(18)F]PBR111, in rat and primate plasma. Nuclear medicine and biology 38:137-148.

Kelly ME, McIntyre DC (1996), Perirhinal cortex involvement in limbic kindled seizures. Epilepsy research 26:233-243.

Kumar A, Chugani HT, Luat A, Asano E, Sood S (2008), Epilepsy surgery in a case of encephalitis: use of 11C-PK11195 positron emission tomography. Pediatric neurology 38:439-442.

Kumlien E, Hilton-Brown P, Spannare B, Gillberg PG (1992), In vitro quantitative autoradiography of [3H]-L-deprenyl and [3H]-PK 11195 binding sites in human epileptic hippocampus. Epilepsia 33:610-617.

Lavisse S, Guillermier M, Herard AS, Petit F, Delahaye M, Van Camp N, Ben Haim L, Lebon V, Remy P, Dolle F, Delzescaux T, Bonvento G, Hantraye P, Escartin C (2012), Reactive astrocytes overexpress TSPO and are detected by TSPO positron emission tomography imaging. The Journal of neuroscience : the official journal of the Society for Neuroscience 32:10809-10818.

Le Fur G, Guilloux F, Rufat P, Benavides J, Uzan A, Renault C, Dubroeucq MC, Gueremy C (1983), Peripheral benzodiazepine binding sites: effect of PK 11195, 1-(2-chlorophenyl)-N-methyl-(1-methylpropyl)-3 isoquinolinecarboxamide. II. In vivo studies. Life sciences 32:1849-1856.

Maia S, Arlicot N, Vierron E, Bodard S, Vergote J, Guilloteau D, Chalon S (2012), Longitudinal and parallel monitoring of neuroinflammation and neurodegeneration in a 6-hydroxydopamine rat model of Parkinson's disease. Synapse 66:573-583.

Martin A, Boisgard R, Theze B, Van Camp N, Kuhnast B, Damont A, Kassiou M, Dolle F, Tavitian B (2010), Evaluation of the PBR/TSPO radioligand [(18)F]DPA-714 in a rat model of focal cerebral ischemia. Journal of cerebral blood flow and metabolism : official journal of the International Society of Cerebral Blood Flow and Metabolism 30:230-241.

Missault S, Van den Eynde K, Vanden Berghe W, Fransen E, Weeren A, Timmermans JP, Kumar-Singh S, Dedeurwaerdere S (2014), The risk for behavioural deficits is determined by the maternal immune response to prenatal immune challenge in a neurodevelopmental model. Brain, behavior, and immunity 42:138-146.

Ngugi AK, Bottomley C, Kleinschmidt I, Sander JW, Newton CR (2010), Estimation of the burden of active and life-time epilepsy: a meta-analytic approach. Epilepsia 51:883-890.

Noda M, Suzumura A (2012), Sweepers in the CNS: Microglial Migration and Phagocytosis in the Alzheimer Disease Pathogenesis. International journal of Alzheimer's disease 2012:891087.

Patel AR, Ritzel R, McCullough LD, Liu F (2013), Microglia and ischemic stroke: a double-edged sword. International journal of physiology, pathophysiology and pharmacology 5:73-90.

Paxinos G, Watson C (2007) The rat brain in stereotaxic coordinates.: Elsevier Inc.

Pike VW, Halldin C, Crouzel C, Barre L, Nutt DJ, Osman S, Shah F, Turton DR, Waters SL (1993), Radioligands for PET studies of central benzodiazepine receptors and PK (peripheral benzodiazepine) binding sites--current status. Nuclear medicine and biology 20:503-525.

Pitkanen A, Nissinen J, Nairismagi J, Lukasiuk K, Grohn OH, Miettinen R, Kauppinen R (2002), Progression of neuronal damage after status epilepticus and during spontaneous seizures in a rat model of temporal lobe epilepsy. Progress in brain research 135:67-83.

Racine RJ (1972), Modification of seizure activity by electrical stimulation. II. Motor seizure. Electroencephalography and clinical neurophysiology 32:281-294.

Ravizza T, Balosso S, Vezzani A (2011), Inflammation and prevention of epileptogenesis. Neuroscience letters 497:223-230.

Ravizza T, Boer K, Redeker S, Spliet WG, van Rijen PC, Troost D, Vezzani A, Aronica E (2006), The IL-1beta system in epilepsy-associated malformations of cortical development. Neurobiology of disease 24:128-143.

Ravizza T, Gagliardi B, Noe F, Boer K, Aronica E, Vezzani A (2008), Innate and adaptive immunity during epileptogenesis and spontaneous seizures: evidence from experimental models and human temporal lobe epilepsy. Neurobiology of disease 29:142-160.

Saijo K, Glass CK (2011), Microglial cell origin and phenotypes in health and disease. Nature reviews Immunology 11:775-787.

Sauvageau A, Desjardins P, Lozeva V, Rose C, Hazell AS, Bouthillier A, Butterwort RF (2002), Increased expression of "peripheral-type" benzodiazepine receptors in human temporal lobe epilepsy: implications for PET imaging of hippocampal sclerosis. Metabolic brain disease 17:3-11.

Sharma AK, Jordan WH, Reams RY, Hall DG, Snyder PW (2008), Temporal profile of clinical signs and histopathologic changes in an F-344 rat model of kainic acid-induced mesial temporal lobe epilepsy. Toxicologic pathology 36:932-943.

Stellwagen D, Beattie EC, Seo JY, Malenka RC (2005), Differential regulation of AMPA receptor and GABA receptor trafficking by tumor necrosis factor-alpha. The Journal of neuroscience : the official journal of the Society for Neuroscience 25:3219-3228.

Van den Eynde K, Missault S, Fransen E, Raeymaekers L, Willems R, Drinkenburg W, Timmermans JP, Kumar-Singh S, Dedeurwaerdere S (2014), Hypolocomotive behaviour associated with increased microglia in a prenatal immune activation model with relevance to schizophrenia. Behavioural brain research 258:179-186.

van Raay L, Morris MJ, Reed RC, O'Brien TJ, Dedeurwaerdere S (2009), A novel system allowing long-term simultaneous video-electroencephalography recording, drug infusion and blood sampling in rats. Journal of neuroscience methods 179:184-190.

Vezzani A, French J, Bartfai T, Baram TZ (2011), The role of inflammation in epilepsy. Nature reviews Neurology 7:31-40.

White A, Williams PA, Hellier JL, Clark S, Dudek FE, Staley KJ (2010), EEG spike activity precedes epilepsy after kainate-induced status epilepticus. Epilepsia 51:371-383.

Williams PA, White AM, Clark S, Ferraro DJ, Swiercz W, Staley KJ, Dudek FE (2009), Development of spontaneous recurrent seizures after kainate-induced status epilepticus. The Journal of neuroscience : the official journal of the Society for Neuroscience 29:2103-2112.

Wittner L, Eross L, Czirjak S, Halasz P, Freund TF, Magloczky Z (2005), Surviving CA1 pyramidal cells receive intact perisomatic inhibitory input in the human epileptic hippocampus. Brain : a journal of neurology 128:138-152.

Zattoni M, Mura ML, Deprez F, Schwendener RA, Engelhardt B, Frei K, Fritschy JM (2011), Brain infiltration of leukocytes contributes to the pathophysiology of temporal lobe epilepsy. The Journal of neuroscience : the official journal of the Society for Neuroscience 31:4037-4050.